A micro bio-inspired teeter-totter velocity sensitive microphone structure

Morteza Karimi,[1,a)] Junpeng Lai,[1] Zihan Liu,[1] Weili Cui,[2] Changhong Ke,[1] and Ronald N. Miles[1,b)]

[1]*Department of Mechanical Engineering, Binghamton University, Binghamton, New York 13902, USA*

[2]*Department of Mechanical & Facility Engineering, School of Engineering, SUNY Maritime College, 6 Pennyfield Avenue, Bronx, New York 10465, USA*

ABSTRACT:

This study experimentally examines the development of a bio-inspired teeter-totter low-noise velocity-sensitive microphone. Several microscale prototypes were constructed using a micromanipulator, microscope, epoxy, super glue, and basic materials. None of the prototypes presented in this article represent a fully optimized, functional device; however, they could demonstrate how the performance of this flow-sensing microphone can be improved. The simplest design features a beam held by a hinge inside a cavity. By modifying this structure, such as altering the hinge material and increasing the beam's surface area (e.g., by adding more beams), the thermal noise floor, acoustic response, phase response, and pressure-referred noise of different samples are measured and compared. The results demonstrate that softening the hinge (by making it thin and flexible), lowering the beam rocking mode frequency, increasing the surface area while maintaining a reasonable structure weight, and keeping the first bending mode of the beam at a higher frequency out of the range of normal hearing significantly improves the sensor's performance. These findings offer valuable insights into designing high-performance, low-noise acoustic particle velocity sensors.
© 2025 Acoustical Society of America. https://doi.org/10.1121/10.0037234

I. INTRODUCTION

The evolution of acoustic sensing mechanisms in nature offers intriguing insights for the development of novel microphone technologies. While traditional microphone design has predominantly drawn inspiration from the pressure-sensing tympanal membranes found in humans and most vertebrates,[1,2] an alternative approach based on acoustic flow detection, as employed by a vast array of hearing animals, presents promising opportunities for innovation. Insects such as mosquitoes and other arthropods, such as spiders, for instance, often utilize thin, viscous-driven hairs to detect sound, responding to velocity (a vector) rather than pressure (a scalar).[3–8] This method not only captures sound but also provides information on the direction of sound propagation, offering a significant advantage over conventional pressure-sensing microphones. The main purpose of the present study is to explore possible ways to fabricate acoustic sensors that take advantage of the sensing principles used in these natural designs.

The parasitoid fly, *Ormia ochracea*, exemplifies an intermediate approach: its tympanal ears, mechanically coupled by a cuticular bridge, enclose a common back volume of air (cavity). This unique structure enables the ears to detect sound pressure gradients related to acoustic flow, producing a directionally dependent tympanal response. As a result, the fly can pinpoint sound sources with remarkable

precision.[9–13] Inspired by these diverse biological solutions, researchers have been exploring biomimetic designs for miniature directional microphones.[14–24] These efforts aimed to overcome the limitations of traditional pressure-gradient detection methods, which typically rely on membrane or diaphragm-like structures. However, the present study aims to create a simple prototype of a velocity-sensitive microphone by combining strategies inspired by the previously mentioned animals. This approach involves developing a novel design consisting of a movable micro-beam supported by a torsional hinge over a volume of air (cavity) using basic materials and equipment, and then experimentally analyzing its response to the thermal noise floor and acoustic stimuli. The design draws inspiration from flow-sensing hairs in spiders and mosquito antennae, as well as the coupled tympanal ears of *Ormia ochracea* flies.

An intriguing example of acoustic flow sensing is observed in orb-weaving spiders, which "outsource" their hearing capabilities through their webs.[25] The movement of a strand of spider silk can mimic the surrounding acoustic particle velocity, allowing the spider to detect sound near the web.[26] While spider silk itself may not be practical for commercial microphones due to durability concerns, this principle has inspired the use of fine hair-like structures in flow sensing. Silicon microfabrication has been employed to create such structures, often mimicking insect flow-sensing hairs with rigid structures supported on flexible hinges.[27,28]

Given the time-consuming and expensive nature of microfabrication, it is essential to carefully analyze the design

---
a)Email: mkarimi3@binghamton.edu
b)Email: miles@binghamton.edu

before proceeding with microfabrication. Therefore, this study focuses on creating a **simple** prototype using basic materials to minimize costs and streamline the development process. The proposed microphone features a movable microbeam supported by a carefully placed torsional hinge on either side, positioned over an air-filled cavity. This setup allows acoustic flow into and out of the cavity to drive the motion of the beam.[29] We will refer to this type of microphone as a "teeter-totter" design microphone. The movable beam is constructed either from carbon fiber, approximately 5 μm in diameter, or from different pieces of silicon structures. The hinge is designed to incorporate materials with different specifications, ranging from carbon fiber with a diameter of 5 μm to a rectangular silicon beam that is 280 nm thick and 5 μm wide. By modifying this structure through the use of different hinge materials and increasing the surface area of the movable beam, this study aims to measure and compare the thermal noise floor, acoustic response, phase response, and pressure-referred noise of various samples.

This research endeavors to experimentally elucidate the steps and directions for developing a bio-inspired-low-noise-velocity-sensitive microphone. It aims to identify effective design parameters for reducing the thermal noise floor while simultaneously increasing the acoustic response, ultimately decreasing pressure-referred noise and enhancing the performance of the teeter-totter velocity-sensitive microphone.

As research in this field progresses, it promises to revolutionize microphone technology, potentially leading to higher performance, directional, and sensitive acoustic sensors that could find applications in various fields, from communications to environmental monitoring.

II. PROCEDURE

In this section, a practical experimental approach was used to develop a bio-inspired teeter-totter velocity-sensitive microphone. Various prototypes were constructed using basic materials, such as carbon fiber and silicon, to identify key design factors that impact microphone performance. This straightforward method enabled the exploration of various design modifications and their impact on performance metrics, offering valuable insights into optimizing the microphone without resorting to complex microfabrication processes. In the following, we outline the experimental procedures and adjustments undertaken in the development of a low-noise velocity-sensitive microphone.

The process started with the simplest version of the microphone that is driven by viscous forces: a beam inside a cavity, which served as the basis for subsequent design refinements. For more detailed information on how this cavity works and the concept of velocity-sensitive microphones, please refer to Ref. 29. The structure in this design should have a first mode in which the structure moves as a rigid body with flexible supports so that its resonant frequency is significantly below the frequency being detected (i.e., approximately 0 Hz). The second structural mode should have a frequency above the frequency range of interest. This second

mode will typically consist of the first flexible bending mode of the structure. This frequency, of course, is dependent on the size and material properties of the beam as described in the following, which allows for adjustability.[30,31] In Eq. (1), E, I, L, and ϱ represent the modulus of elasticity, area moment of inertia, beam length, and density, respectively. For this microphone design, we would first like the natural frequency to be as low as possible (around 0 Hz, or at least well below the frequency range of hearing) while also keeping the mass of the moving structure as small as possible. The result will be a highly compliant structure, enabling it to respond to sound. To minimize the response to thermal noise, it is desirable to also minimize the number of resonant modes in the audible frequency range. The second beam mode should then have a frequency exceeding the hearing range at more than 20 kHz. However, in a practical design, the beam cannot remain entirely free, having a first natural frequency of zero Hertz, since this would make it highly vulnerable to damage due to being dropped. Therefore, incorporating a hinge mechanism is necessary to support and stabilize the free-free beam. By attaching a hinge to the beam, the first beam mode now depends on the rotational stiffness of the hinge, as described in the following.[30,31] This mode is known as the "teeter-totter" or "rocking" mode of the beam. For clarity, the first beam mode is hereafter referred to as the "rocking mode," and the second beam mode as the "first beam bending mode."

In Eq. (2), G, J, and L represent the shear modulus, polar moment of inertia, and length of hinge, respectively.

To demonstrate the noise floor and acoustic response of this simple microphone, a sample was created incorporating the features outlined in Fig. 1. In this sample, a cavity was constructed with dimensions of 1300 μm in length, 900 μm in width, and 500 μm in depth. A carbon fiber with a diameter of 5 μm was chosen to serve both as the beam and the hinge within this cavity structure. The carbon fiber has a modulus of elasticity $E = 170$ GPa and a density $\varrho = 1500$ kg/m^3. The dimensions of the beam are diameter $d = 5$ μm and length $L = 1250$ μm, and for the hinge, diameter $d = 5$ μm and length $L = 900$ μm.

The construction of this sample was accomplished utilizing a model 525 Micromanipulator (The Micromanipulator Company, Carson City, NV), a Leica WILD M3Z Stereo Zoom Microscope (Leica Microsystems, Wetzlar, Germany), a Zeiss AxioSkop-40 microscope (Zeiss, Oberkochen, Germany), epoxy, and super glue. The carbon fiber hinge was securely glued to both sides of the cavity along the width, and the beam was then glued to the middle of the hinge along the length. This setup resulted in a system with one free degree of freedom, allowing for controlled movement and response within the microphone structure.

$$f_1 = 0, \quad (Rigid\,Body\,Mode)$$

$$f_2 = \frac{1}{2\pi}\left(\frac{22.373}{L^2}\right)\sqrt{\frac{EI}{\varrho}}, \quad (Bending\,Mode\,of\,the\,Beam),$$

(1)

J. Acoust. Soc. Am. **158** (2), August 2025
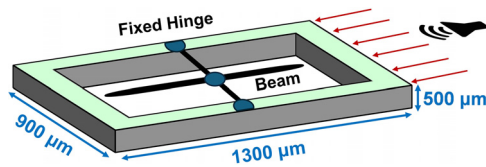
Karimi *et al.*   901

FIG. 2. The schematic of the sample, with two carbon fibers serving as hinge and beam elements, assembled within a specified cavity. Note that this structure is placed on a smooth, flat surface so that only the top of the cavity is exposed to sound.

$$\text{K} = \frac{GJ}{L}, \quad (\textit{Tortional stiffness of the Hinge}). \quad (2)$$

Figure 2 presents a schematic diagram of the sample configuration, illustrating two carbon fibers that function as both hinge and beam elements. The schematic depicts their assembly within a designated cavity. To drive the movable beam, a plane wave sound field is generated by a loudspeaker 3 meters away from the side of the cavity. This schematic diagram allows for a comprehensive understanding of the sample's structure and the mechanism by which it operates.

Figure 3 illustrates the noise floor and acoustic measurement setup, which includes key components such as a Polytec OFV-534 laser vibrometer, a B&K type 4138 1/8 in. reference microphone, and motorized stages for precise positioning.

In the acoustic measurement, a stimulus signal is generated using MATLAB and transmitted through a National Instruments PXI 1033 data acquisition system. This signal is processed by a dbx model 234xs crossover filter, which separates it into low-, mid-, and high-frequency bands. These bands are amplified by Crown D-75 (Crown Audio, Elkhart, IN) and Techron 5530 (Techron, San Ramon, CA) amplifiers and directed to the corresponding woofer, midrange, and tweeter components of a speaker placed 3 meters away from the test location. A B&K type 4138 microphone captures the resulting sound pressure, and its signal is amplified using a B&K type 5935 L dual microphone power supply. Simultaneously, a laser vibrometer measures the velocity

response of the test sample, with all data acquired by the PXI 1033 system (Apex Waves, Cary, NY).

To determine the air velocity used in the acoustic and phase response analysis, a plane wave assumption is applied. Under this assumption, the relationship between acoustic pressure and particle velocity is given by $u = p/(\varrho_0 c_0)$, where u is the particle velocity, p is the pressure measured by the reference microphone, ϱ_0 is the ambient air density, and c_0 is the speed of sound in air. This formulation assumes linear, one-dimensional wave propagation, which is valid in the frequency range and spatial configuration of the measurement setup. The pressure measurement from the reference microphone serves as the input for calculating air velocity across the acoustic frequency range.

Having time domain signals for the acoustic particle velocity (from the reference microphone measurement as described previously) and the velocity signal obtained from our laser vibrometer, we obtained a complex transfer function in the frequency domain by the use of a digital fast Fourier transform (FFT).[31] This approach ensures that the sensor's output is consistently compared against a well-defined acoustic input. This approach ensures that the sensor's output is consistently compared against a well-defined acoustic input.

Thermal noise floor measurements are obtained by capturing sample velocity due to ambient thermal excitation, in the absence of an external acoustic stimulus. This data is likewise acquired using the PXI system and processed in MATLAB. The pressure-referred noise (PRN) is computed as the ratio of thermally driven mechanical velocity to the sensor's acoustic pressure response, scaled by the acoustic impedance. This figure of merit, calculated over the audio frequency range from 100 Hz to 40 kHz and A-weighted, offers insight into the sensor's sensitivity performance.

For more information about how to measure the thermal noise floor and acoustic response, please refer to Ref. 32. This setup is used for all subsequent measurements of the thermal noise floor and acoustic response, with the sample positioned horizontally on a glass surface unless stated otherwise. This orientation ensures that the backside of the cavity is closed.
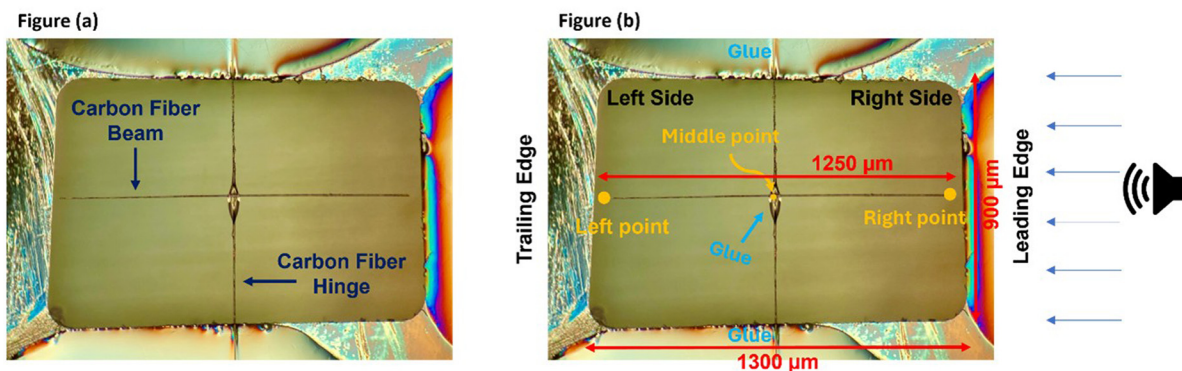

FIG. 1. Indicates the simplest teeter-totter microphone design featuring two carbon fibers serving as both hinge and beam elements, showing their assembly within a specified cavity. The figures show a plan view of the cavity as viewed from above the cavity opening. Sound arriving from the right will cause oscillatory flow (into the page) at the leading edge with out-of-phase flow at the trailing edge. (a) Shows the design without dimensions, while (b) includes detailed dimensions.
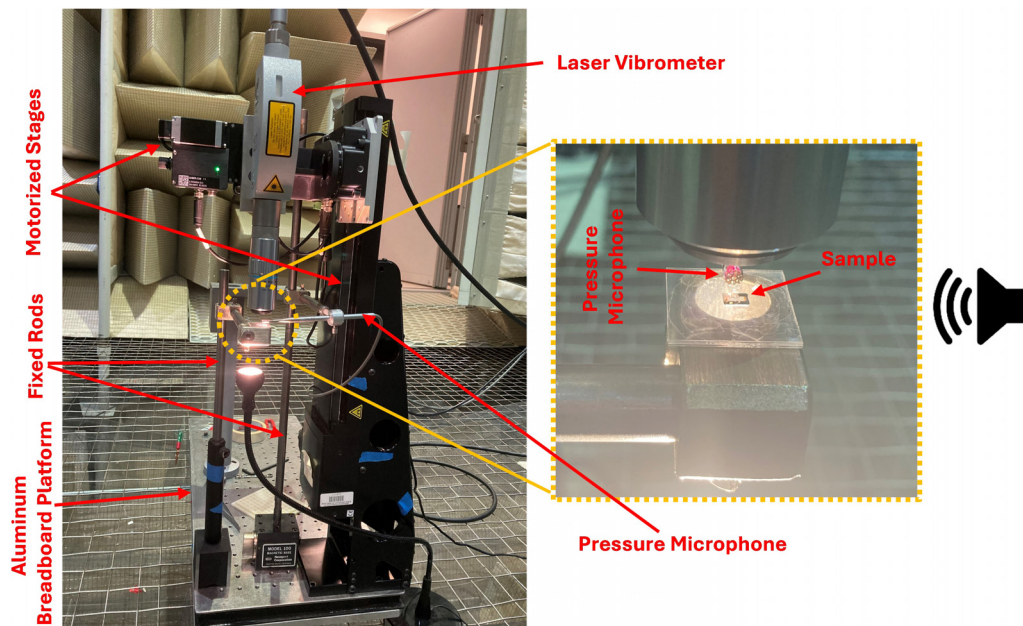
FIG. 3. The noise floor and acoustic setup, including its components for measurement and sample positioning. The system includes a Polytec OFV-534 laser vibrometer (Polytec, Los Angeles, CA), a B&K type 4138 reference microphone (Brüel & Kjaer, Naerum, Denmark), and motorized stages, an aluminum breadboard platform, and fixed rods where the sample is placed. This setup is designed for precise measurement of sound pressure, sample velocity, and thermal noise floor, with signals processed and amplified through a crossover filter and amplifiers for testing acoustic response.

Figures 4(a)–4(c) depict (a) thermal noise floor response, (b) acoustic response, and (c) phase response of the simple teeter-totter microphone constructed with carbon fiber for both the beam and hinge within the cavity structure, across various frequencies. The frequency range for the thermal noise floor spans from 100 Hz to 100 kHz to capture all relevant modes. However, the acoustic response focuses specifically on the frequency range from 100 Hz to 10 kHz, which is of primary interest. Based on Fig. 4(a), it is evident that the left (represented by the symbol ●) and right (represented by the symbol ✖) sides of the beam exhibit similar responses, indicating that the structure is well-made and symmetrical. Additionally, measuring the response at the middle point (represented by the symbol ⬠) of the beam helps us understand whether the second mode is attributed to the entire structure moving up or down (first hinge bending mode), or if it originates from the first beam bending mode itself. If the mode observed at both ends of the movable beam occurs at the same level as the mode at the middle point, it can be concluded that this mode is a result of the entire structure moving up and down (first hinge bending mode). The base or chip (represented by the symbol **B**) refers to the measurement point on the fixed chip used as a reference. The base outcome presented in this figure is intended to illustrate the comparison between the responses of the movable beam and its fixed chip. Several modes observed in the base results are attributed to electromagnetic noise in the instrumentation. For instance, the mode at 380 Hz appears not only in the base measurement but also in other plots, suggesting that this mode originates from electromagnetic interference or other external factors rather than from the structure or the sensing element itself.

The first natural frequency of the carbon fiber beam measures around 6 kHz, while the second natural frequency is approximately 24 kHz. Since the modes at the ends of the beam are not at the same level as the mode at the middle point, the first mode can be identified as the rocking mode of the movable beam, and the second mode as the first bending mode of the movable beam. The third mode occurs at 80 kHz, which is observed at both ends of the beam and the middle point. This indicates that the third mode is the mode where the entire structure moves up and down, known as the first bending mode of the hinge.

From the data shown in Fig. 4(b), it is clear that both sides of the beam display comparable response, reinforcing the notion that the structure is well-constructed and balanced. Also, it appears that the response to sound at low frequencies is not satisfactory, primarily due to the driving mode of the structure occurring at a higher frequency, approximately 6 kHz. The phenomenon described is also depicted in Fig. 4(c), where the phase response of the structure indicates that there is no movement until a frequency of 300 Hz is reached. Beyond this frequency, it becomes apparent that the left and right sides of the beam are out of phase. This means that sound enters the cavity through the right side (Leading Edge) and exits through the left side (Trailing Edge) of the structure. This phase difference illustrates how the structure interacts with sound waves at different frequencies, particularly highlighting the behavior of sound propagation within the cavity. For more detailed information on how the cavity works, please refer to Ref. 29.

From the results shown in Fig. 4, it can be concluded that reducing the frequency of the beam rocking mode is beneficial for several reasons. By lowering the frequency of

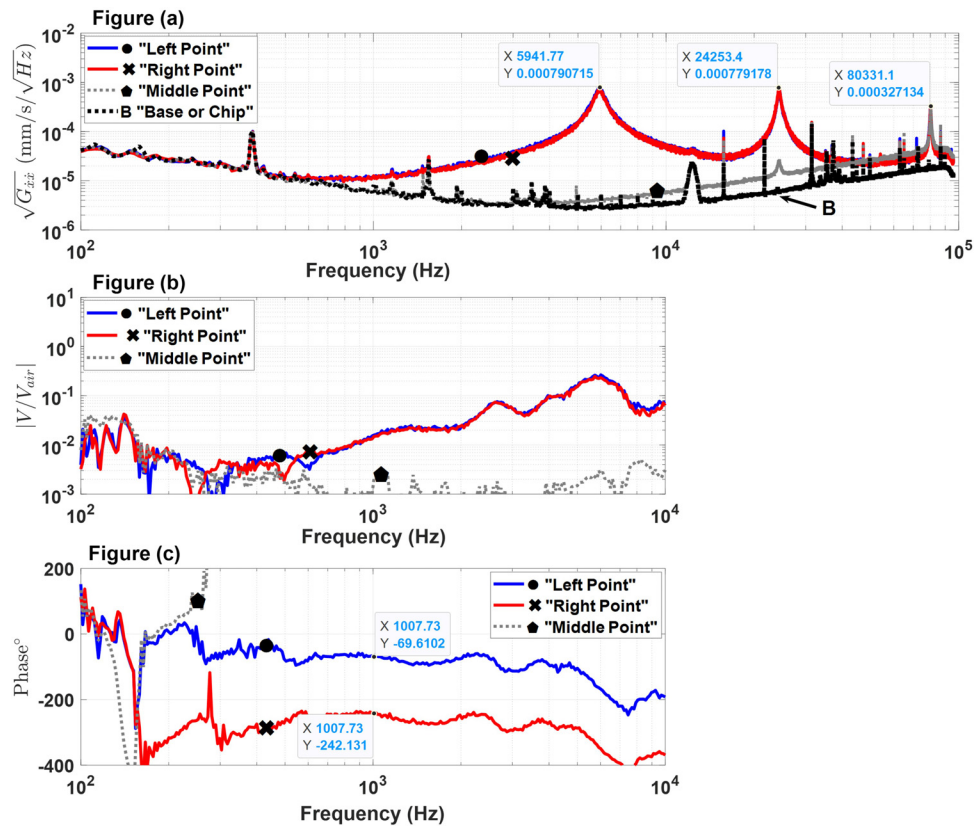J. Acoust. Soc. Am. **158** (2), August 2025

Karimi *et al.*   903

FIG. 4. (a) Thermal noise floor response, (b) acoustic response, and (c) phase response of a teeter-totter microphone designed with carbon fiber for both the beam and hinge within the cavity structure, measured across various frequencies. The vertical axis for (a) represents the velocity of the beam per square root of frequency, $\sqrt{G_{\dot{x}\dot{x}}}$ (mm/s/$\sqrt{\text{Hz}}$), (b) shows the ratio of the beam velocity to the air velocity, $V_{\text{beam}}/V_{\text{air}}$ (unitless), and (c) represents the phase in degrees.

the rocking mode, the separation between the rocking and first beam bending modes increases, creating a deeper canyon between these modes. This separation results in a decreased thermal noise floor and shifts the rocking mode out of the hearing range (ideally below 20 Hz, as the audible frequency range for humans typically falls between 20 Hz and 20 kHz), enhancing the overall performance of the structure. Additionally, lowering the frequency of the rocking mode improves the structure's response to sound because this mode is the driving mode. Therefore, optimizing the frequency of the rocking mode can lead to better efficiency and effectiveness in responding to sound stimuli. This

adjustment aligns with improving the structure's performance and functionality based on the observed data, which will be examined in detail in the following steps.

A. Step 1: Reducing the rocking mode frequency

To lower the rocking mode, using a softer hinge by making it thin and flexible could be a solution since the dominant motion involves rotation at the hinge. Therefore, a new sample with a softer rotation hinge has been created. Figure 5 depicts another simple teeter-totter microphone with a significantly softer and thinner hinge compared to the
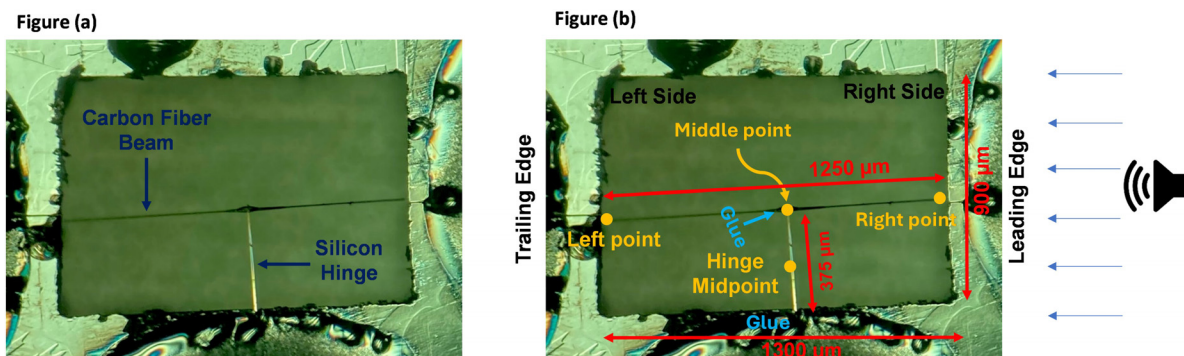

FIG. 5. Indicates the simplest teeter-totter microphone design featuring a carbon fiber beam as the movable element and a silicon structure as the hinge, demonstrating their assembly within a specified cavity. (a) shows the design without dimensions, while (b) includes detailed dimensions.

904   J. Acoust. Soc. Am. **158** (2), August 2025
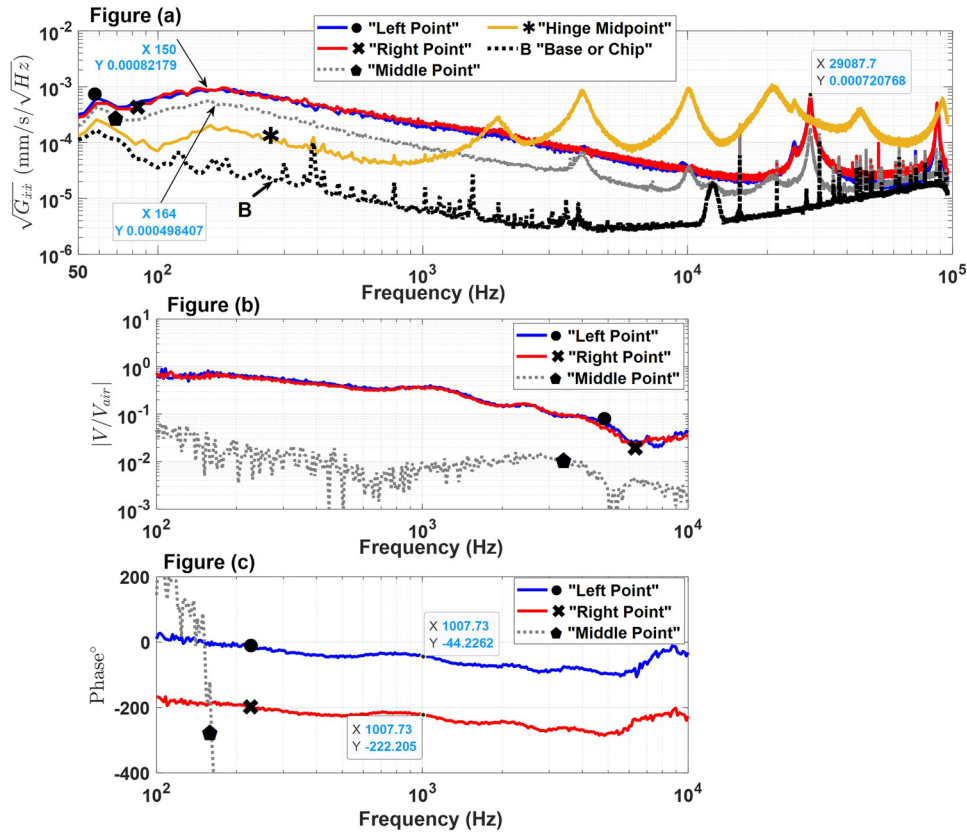
Karimi et al.

FIG. 6. Illustrates the (a) thermal noise floor response, (b) acoustic response, and (c) phase response of a teeter-totter microphone designed with carbon fiber beam as the movable element and a silicon structure as the hinge within the cavity structure, across various frequencies.

carbon fiber hinge. The dimensions of this softer and thinner hinge are as follows: width $w = 5\,\mu m$, length $L = 375\,\mu m$, and thickness $h = 280\,nm$. The carbon fiber beam and cavity size remain consistent to allow for a meaningful comparison between the two structures, with the hinge support being the sole point of differentiation.

Figures 6(a)–6(c) illustrate the (a) thermal noise floor response, (b) acoustic response, and (c) phase response of a teeter-totter microphone design featuring a carbon fiber beam as the movable element and a silicon hinge within the cavity structure, across various frequencies. The thermal noise floor data covers a frequency range from 50 Hz to 100 kHz to encompass all relevant modes. In contrast, the acoustic response focuses specifically on frequencies from 100 Hz to 10 kHz, which are of primary interest. To facilitate a comparison between the experimental results depicted in Fig. 6 and those obtained from finite element method (FEM) simulations, Fig. 7 presents the COMSOL simulation

FIG. 7. Presents the COMSOL results depicting the mode shape and natural frequency of a teeter-totter microphone, featuring a carbon fiber beam as the movable element and a silicon structure serving as the hinge.

results showcasing the mode shape and natural frequency of a teeter-totter microphone. The material properties and dimensions of the carbon fiber beam are as follows: modulus of elasticity $E = 170$ GPa, density $\varrho = 2270$ kg/m^3, diameter $d = 5\,\mu$m, and length $L = 1250\,\mu$m. For the silicon hinge, the properties and dimensions are: modulus of elasticity $E = 170$ GPa, density $\varrho = 2329$ kg/m^3, width $w = 5\,\mu$m, length $L = 375\,\mu$m, and thickness $h = 280$ nm.

The base or chip (represented by the symbol B) in Fig. 6(a) refers to the measurement point on the fixed chip used as a reference to compare the responses of the movable beam and the fixed structure. As in previous observations, several modes in the base results—such as the 60 Hz peak—are likely due to electromagnetic noise in the instrumentation rather than originating from the structure or the sensing element.

Upon analyzing Fig. 6(a), it is evident that both the left (represented by the symbol ●) and right (represented by the symbol ✖) sides of the beam show similar responses, indicating excellent symmetry and construction quality. The rocking mode of the carbon fiber beam is around 150 Hz. Moreover, this value based on Fig. 7 is around 151.6 Hz, which is quite close to the experimental result. The gray dotted line curve (represented by the symbol ⬠) indicates the noise floor measurement at the middle point of the movable carbon fiber beam, where it is attached to the silicon hinge. Based on the results, it is observed that around a frequency of 164 Hz, the entire structure undergoes an up-and-down movement corresponding to the first bending mode of the silicon hinge. In the COMSOL model, this frequency value is around 203.2 Hz, which is almost close to the experimental result. It is important to note that these samples are **handmade**, leading to a mismatch between the COMSOL model and the model used for measurement. The second hinge bending mode in the experimental result is around 10 kHz, whereas in COMSOL, it is approximately 12.3 kHz. This mode is also evident from the yellow curve (represented by the symbol ✳), which shows the measurement at the midpoint of the hinge. Another interesting mode occurs around 29 kHz, which is the second bending mode of the carbon fiber beam (shown in the left ● and Right ✖ curves). The COMSOL result for this mode is approximately 26.1 kHz, showing almost good agreement with measurement. Additionally, the Third bending mode of the hinge, observed in the yellow curve, is around 45 kHz, matching closely with the COMSOL result of around 44.3 kHz, showing good agreement. Furthermore, the third bending mode of the carbon fiber beam, observed in the left ● and right ✖ curves, is around 87 kHz, while in the COMSOL model, it is predicted to be 72.8 kHz. There is another mode on the gray dotted line curve ⬠ (beam middle point) around 4 kHz and several modes on the yellow curve ✳ (hinge midpoint) around 2 kHz, 4 kHz, and 21 kHz that were not explained. It should be noted that the laser measures the out-of-plane modes of the structure and should not measure in-plane modes. According to COMSOL simulations, this structure also has some in-plane modes, but these are not included here. Since

the structure is handmade and not perfectly symmetric, these in-plane modes may slightly convert to out-of-plane modes, which the laser vibrometer can then detect them, as shown in Fig. 6(a).

In Fig. 6(b), it is clear that both sides of the beam exhibit similar responses across the 100 Hz to 10 kHz range, confirming that the structure is well-constructed and balanced. Additionally, the structure responds effectively to low-frequency sounds, likely because the driving mode occurs at a relatively low frequency of approximately 150 Hz.

Figure 6(c) shows the phase response of the structure, indicating that the left ● and right ✖ sides of the beam are out of phase from 100 Hz to 10 kHz. This phase difference again means that sound enters the cavity through the right side (Leading Edge) and exits through the left side (Trailing Edge) of the structure.

To compare the results before and after softening the hinge by using a thinner and more flexible design (Figs. 4 and 6), Fig. 8 was generated. Before diving into the analysis, it is important to understand pressure-referred noise (PRN). PRN is a crucial metric that quantifies the sensor's ability to detect faint sounds, a key attribute for sound detection across a broad range of levels. This sensitivity is defined as "minimum detectable pressure" (MDP), or equivalently, PRN. The performance of velocity-sensitive acoustic sensors is significantly influenced by how they respond to thermal noise within the medium. PRN is derived from the ratio of mechanical thermal noise to the acoustic pressure response. While both thermal mechanical noise and acoustic response are frequency-dependent, PRN remains largely frequency-independent. It is calculated as the ratio of mechanical thermal noise to the acoustic pressure response of the sensor, multiplied by the acoustic impedance Z, as expressed in Eq. (3),

$$\sqrt{G_{PP}} = PRN = \frac{Thermal\,Noise\,Floor}{Acoustic\,Response} \times Z$$
$$= \frac{V_{beam}/\sqrt{Hz}}{V_{beam}/V_{air}} \times Z$$
$$Z = \frac{P}{V_{air}} = \varrho c. \tag{3}$$

Here, $\sqrt{G_{pp}}$ represents PRN in units of (Pa/$\sqrt{Hz}$). P denotes pressure, ϱ is the density of the medium, and c represents the speed of sound in that medium. PRN's relative consistency across the audible spectrum is attributed to its dependence on the inherent characteristics of the microphone's internal components—like electronic noise from amplifiers or thermal noise from resistors—and the acoustic impedance of the medium, rather than the frequency of the sound detected.

Figure 8(a) illustrates the thermal noise floor, Fig. 8(b) the acoustic response, and Fig. 8(c) the pressure-referred noise for two previously evaluated samples over a range of frequencies. Only the left-side data of each sample were used for this comparison due to the symmetrical nature of the responses on both sides.

In Fig. 8(a), a comparison between the blue curve (representing a design with carbon fiber for both the movable beam and hinge, indicated by a ■) and the red curve
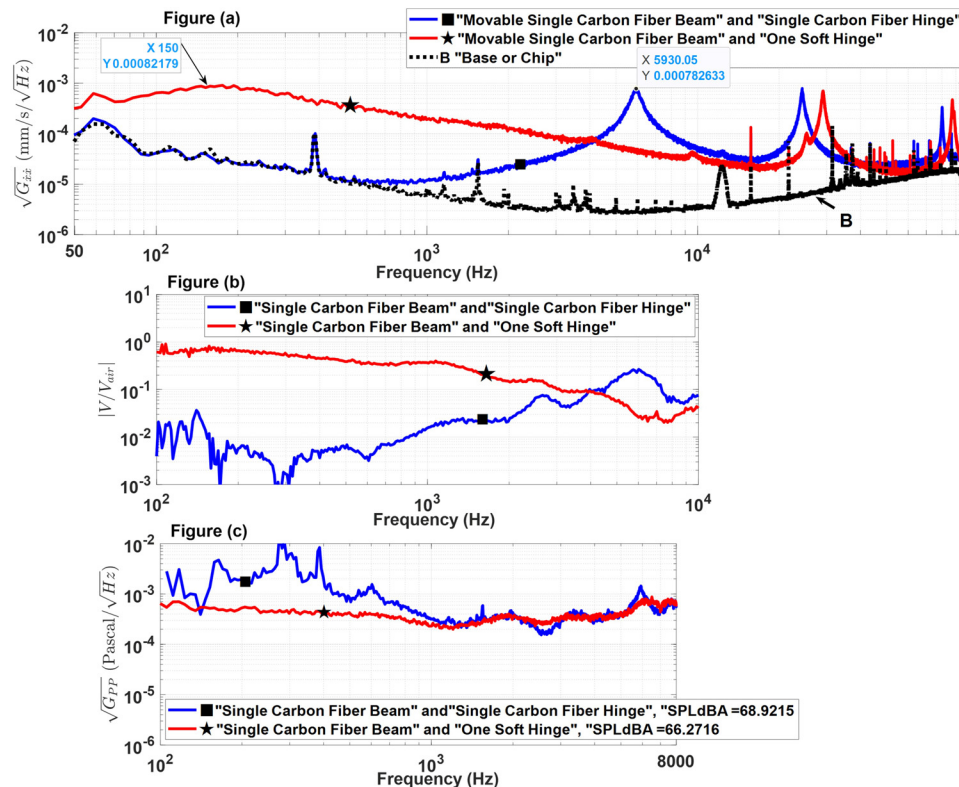
FIG. 8. Illustrates the (a) thermal noise floor response, (b) acoustic response, and (c) pressure-referred noise for two previously analyzed samples across various frequencies. The blue curve (■) represents the results for the sample with a "movable single carbon fiber beam" and a "single carbon fiber hinge." In contrast, the red curve (★) shows the results for the sample with a soft hinge configuration, consisting of a "movable single carbon fiber beam" and "one soft hinge."

(showing a design with carbon fiber for the movable beam and a very thin silicon hinge, marked by a ★) reveals that softening the hinge, by making it thinner, considerably lowers the rocking mode frequency. The first beam bending mode, influenced by the beam's size and material properties, which remain consistent between the two designs, shows minimal change in frequency. The shift in the rocking mode frequency leads to an increase in the thermal noise floor within the frequency range of 50 Hz to 5 kHz. For better understanding and a complete evaluation of the hinge softening effect, PRN comparisons are essential.

Figure 8(b) shows that, when comparing the blue curve (■) with the red curve (★), softening the hinge to lower the rocking mode frequency significantly amplifies the sensor's response to sound, especially at lower frequencies where the rocking mode is most dominant.

Figure 8(c) displays the pressure-referred noise for the two designs across various frequencies. Comparing the blue curve (■) with the red curve (★), the PRN is observed to be 68.9 sound pressure level (SPL)dBA for the blue curve and 66.2 SPLdBA for the red curve—a reduction of about 2.7 dBA. This decrease reflects a performance improvement in the teeter-totter microphone designs.

In summary, the use of a soft hinge lowers the rocking mode frequency and enhances the acoustic response. However, the issue of an elevated thermal noise floor level persists and will be addressed in subsequent steps.

B. Useful technique: Signal subtraction in data analysis

Before addressing the increased thermal noise floor level, it is essential to clarify the confusion between the rocking mode of the carbon fiber beam and the first bending mode of the silicon hinge—since both occur at similar frequencies—a precise approach is required. The method commonly employed by optics professionals to isolate specific signals and eliminate unwanted ones is applied here.

Figure 9(a) illustrates the actual thermal noise floor setup, including the two laser vibrometers and other necessary components for accurately measuring the left and right points of the beam. Figure 9(b) zooms in to show a schematic of the sample mounted on the fixed rod, highlighting how the left and right points are measured by the laser vibrometers. In the schematic, the laser lenses and fixed rod are scaled down to focus on the sample itself.

As illustrated in Fig. 9, the sample was mounted vertically on the noise floor setup, with two laser vibrometers used to measure the thermal noise floor at the left and right points of the movable beam simultaneously. In this method, as the left side of the beam moves up and one laser measures that point, the right side moves down, and the other laser measures this point. This movement is a result of the inherent dynamics of these teeter-totter samples. Since the two points move in opposite directions, subtracting their signals in the time domain will result in

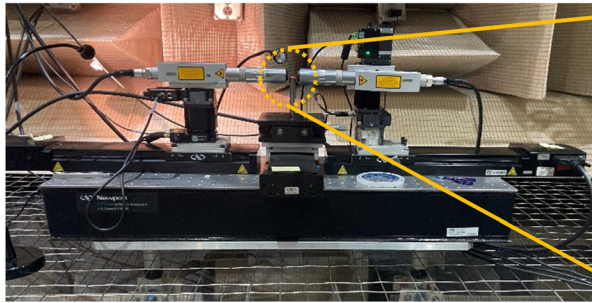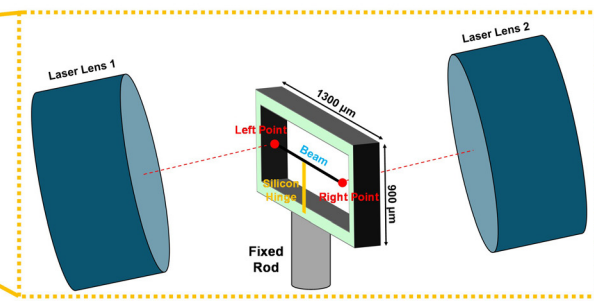FIG. 9. Depicts (a) thermal noise floor measurement setup with laser vibrometers; (b) schematic of sample mounting and measurement points.

the signals doubling if the mode is rocking. Conversely, if the mode is the bending mode of the silicon hinge, where the hinge midpoint moves in one direction, both lasers will measure movement in the same direction. Subtracting these signals would cancel each other out. By subtracting the left and right signals in the time domain and then dividing by two, the actual rocking mode can be detected, while the unwanted bending mode of the hinge is effectively canceled out.

Figure 10 illustrates the subtraction of left and right thermal noise floor signals in a teeter-totter microphone. Like before, the left point is represented by the symbol ●, and the right one is represented by the symbol ✖. This microphone, previously examined in Step 1, features a carbon fiber beam as the movable element and a silicon structure as the hinge within the cavity structure. The measurements were taken across various frequencies using two lasers mounted on the setup to capture data from the left (blue curve ●) and right (red curve ✖) points of the movable beam. The yellow curve (indicated by the symbol Ⓢ) represents the subtraction of the left and right signals in the time domain. Notably, at 150 Hz, the level of thermal noise floor, corresponding to the rocking mode of the beam, nearly doubles in the yellow curve Ⓢ. Conversely, the peak at 60 Hz is effectively canceled out in the yellow curve, indicating that it represents unwanted noise.

This signal subtraction technique proves valuable for extracting meaningful data from noisy signals while simultaneously removing unwanted components. By employing this method, we can isolate and analyze the most relevant aspects of the microphone's performance, enhancing the accuracy and reliability of our findings.

C. Step 2: Reducing the thermal noise floor level

The noise floor level is still not ideal and needs to be lowered. Based on the equations and information in references,[27,31] increasing the damping of the structure would decrease the noise floor level. This means that the interaction between air molecules and the structure must be increased to enhance the damping effect of the viscous force. One way to achieve this is by increasing the surface area of the structure. In this section, movable carbon fiber beams are added based on Figs. 11(a)–11(d) to a carbon fiber hinge within the cavity structure, and the thermal noise floor is measured each time to compare how increasing the surface area affects the noise floor level.

Figure 12 shows the thermal noise floor response as several carbon fiber beams are added incrementally to the carbon fiber hinge of a teeter-totter microphone within a cavity, across various frequencies. In Fig. 12, the blue curve corresponds to one beam on the carbon fiber hinge, represented by symbol ①, with the rocking mode occurring at 5.1 kHz, as depicted in Fig. 11(a). The red curve illustrates three beams on the hinge, represented by symbol ③, with the rocking mode at 3.4 kHz, as shown in Fig. 11(b). The green curve showcases five beams on the hinge, represented by symbol ⑤, with the rocking mode at 3.2 kHz, as presented in Fig. 11(c). Finally, the yellow curve demonstrates all movable beams connected at the end with a stiffener, represented by symbol Ⓜ, where five represents the five beams and S represents the stiffener, indicating a rocking mode at 1.3 kHz, as seen in Fig. 11(d). The gray dotted curve shows the measurement at the middle of the hinge, represented by Ⓜ, as shown in Fig. 11(d). Based on Fig. 12, it is apparent
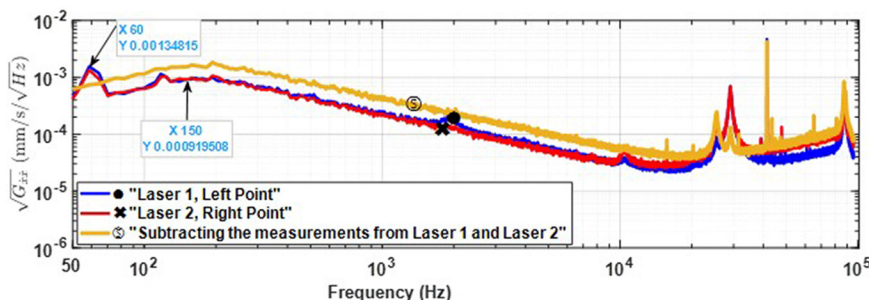

FIG. 10. Shows subtraction of left and right thermal noise floor signals from a teeter-totter microphone, featuring a carbon fiber beam as the movable element and a silicon structure as the hinge, across various frequencies.
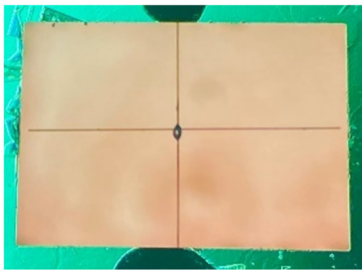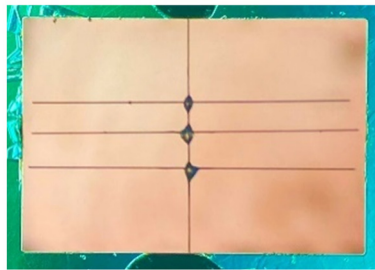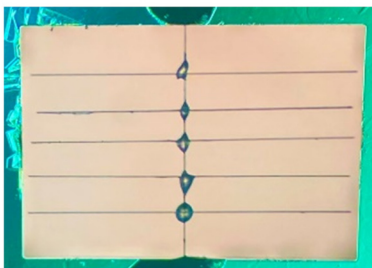
Figure (a): 1 Beam
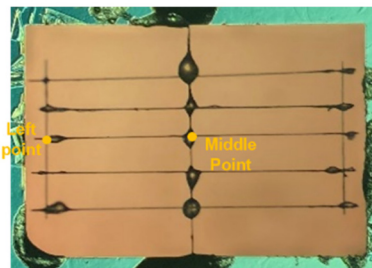
Figure (b): 3 Beams

FIG. 11. Indicates adding several carbon fiber beams on the carbon fiber hinge to indicate the effects of viscous damping on a teeter-totter microphone: (a) 1 beam, (b) 3 beams, (c) 5 beams, and (d) adding stiffeners at the end of movable beams.

Figure (c): 5 Beams

Figure (d): Adding Stiffeners

that adding beams decreases the noise floor level for the rocking mode of the beam, from around 7.3×10^{-4} (mm/s/$\sqrt{Hz}$) to 1.9×10^{-4} (mm/s/$\sqrt{Hz}$), which is almost a four times reduction. This suggests that increasing the surface area by adding beams to the hinge enhances the interaction between air molecules and the structure, consequently increasing damping due to viscous forces. Additionally, adding beams to the hinge introduces multiple degrees of freedom, suggesting that the beams are decoupled and leading to the emergence of additional modes. To couple the beams, one approach is to attach all beams at the end of the movable beams with a stiffener on both sides. This ensures that all beams move together, consolidating the system into one degree of freedom. The yellow curve demonstrates this phenomenon and indicates that the movable beams are coupled, thereby eliminating other extra modes, which are undesirable. There are some extra modes that have appeared on the yellow curve. By comparing the yellow curve with the green curve (5S), which represents the noise floor response of the middle point corresponding to Fig. 11(d), it can be concluded that these extra modes originate from the hinge, indicating that the system is coupled and has one degree of freedom.

Another point to explain from this figure is that by adding more beams to the hinge, the rocking mode occurs at a lower frequency. This is because increasing the number of beams adds weight to the structure, resulting in the rocking mode occurring at a lower frequency, in accordance with the equation $\omega_0 = \sqrt{k/m}$, which governs the relationship between natural frequency (ω_0), stiffness (k), and mass (m).

D. Step 3: Integrating soft hinge with enhanced surface area

1. First prototype

Up to this point, it is evident that reducing the rocking mode of the beam to a lower frequency requires the use of a soft hinge. Additionally, decreasing the level of the thermal noise floor necessitates increasing the damping of the structure by enlarging its surface area. Moreover, maintaining the structure in one degree of freedom is crucial to prevent the occurrence of unwanted extra modes. Therefore, by combining these procedures, utilizing a soft hinge, increasing surface area, and maintaining one degree of freedom, a low-level noise floor can be achieved. Figure 13 depicts a teeter-totter
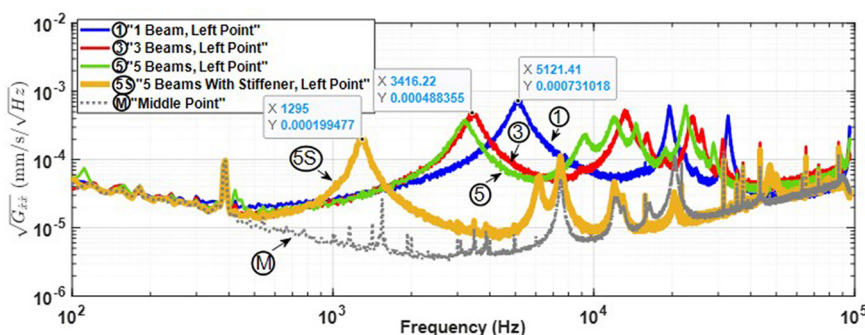

FIG. 12. Illustrates the thermal noise floor response of adding several carbon fiber beams on the carbon fiber hinge for a teeter-totter microphone withing a cavity, across various frequencies.

J. Acoust. Soc. Am. **158** (2), August 2025
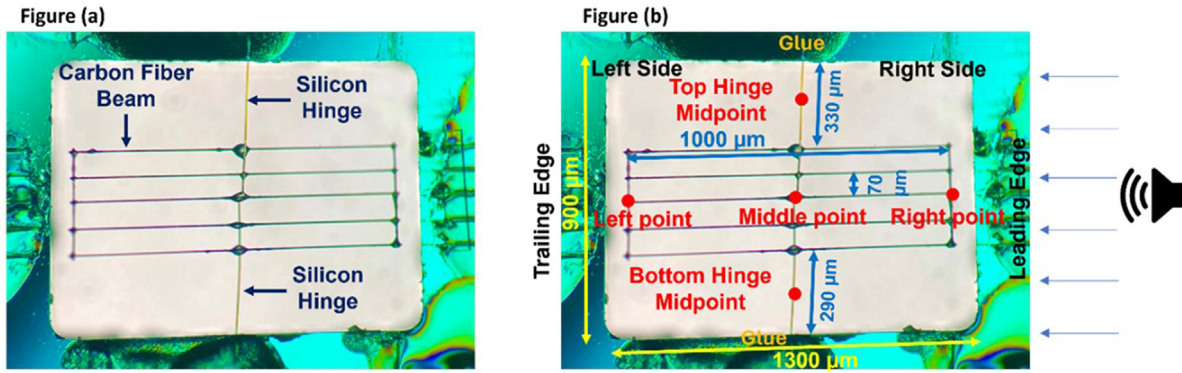
Karimi *et al.* 909

FIG. 13. Depicts a teeter-totter microphone design comprising five carbon fiber beams as the movable elements, coupled at both sides with a stiffener, and silicon structures serving as the hinges on the top and bottom of the cavity, showcased within a specified cavity. (a) Presents the design without dimensions, while (b) includes detailed dimension specifications.

microphone design featuring five carbon fiber beams as the movable element and a silicon structure as the soft hinge within a specified cavity. Both sides of the movable beams are coupled with carbon fiber as a stiffener to prevent the occurrence of extra modes. The carbon fiber beams, silicon hinge, and cavity size remain consistent to ensure meaningful comparisons between all samples made thus far.

Figures 14(a), 14(b), and 14(c) illustrate thermal noise floor response, acoustic response, and phase response of the teeter-totter microphone, respectively, across different frequencies. This design features a movable element composed of five carbon fiber beams, reinforced on both sides with a stiffener and integrated with silicon hinges within the cavity structure. The thermal noise floor data spans a frequency range from 50 Hz to 100 kHz to capture all relevant modes, whereas the acoustic response data focuses on the 100 Hz to 10 kHz range, which is of primary interest. For comparative analysis, Fig. 15 presents the COMSOL simulation results, showing the mode shapes and natural frequencies of the teeter-totter microphone. The material properties and
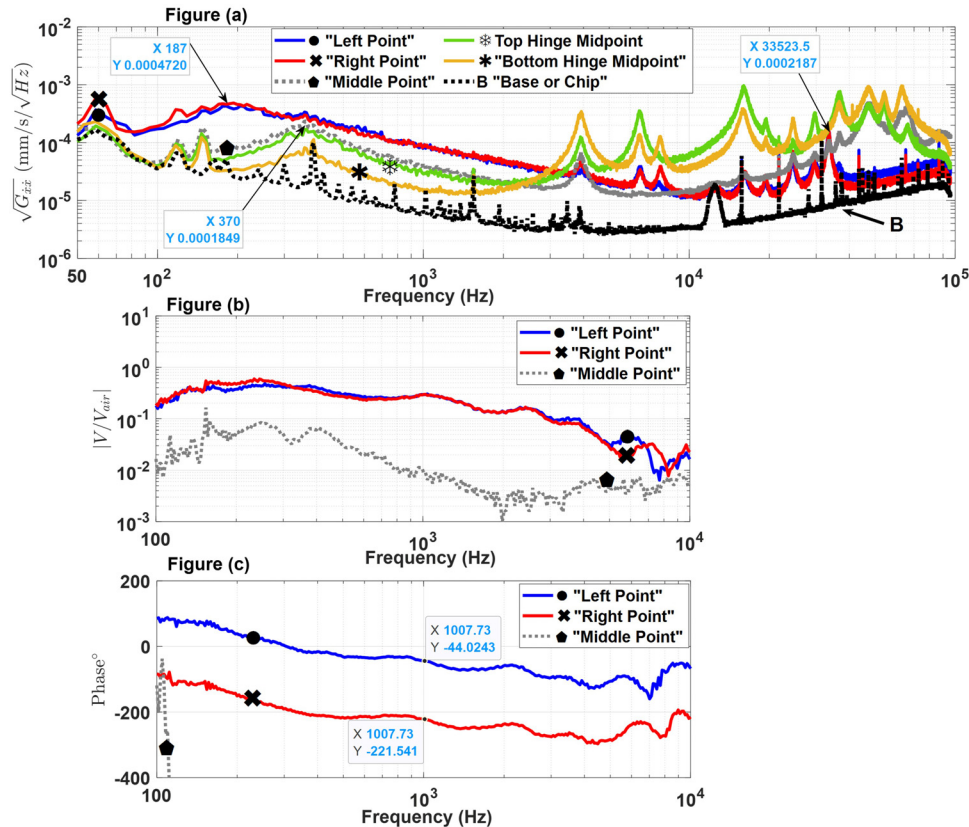

FIG. 14. Illustrates the (a) thermal noise floor response, (b) acoustic response, and (c) phase response of a teeter-totter microphone design comprising five carbon fiber beams as the movable elements, coupled at both sides with a stiffener, and a silicon structure serving as the hinge within a specified cavity, across various frequencies.
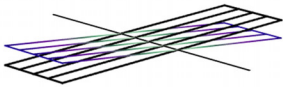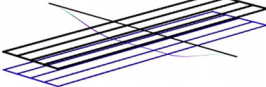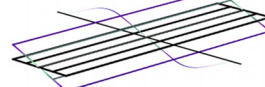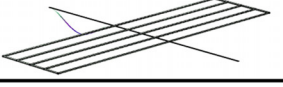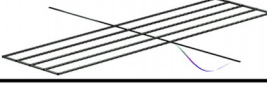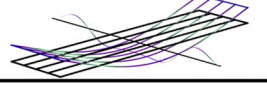
FIG. 15. Presents the COMSOL results depicting the mode shape and natural frequency of a teeter-totter microphone, featuring five carbon fiber beams as the movable element and two silicon hinges.

dimensions for the carbon fiber beams are as follows: modulus of elasticity $E = 170$ GPa, density $\varrho = 2270$ kg/m^3, diameter $d = 5\,\mu$m, and length $L = 1000\,\mu$m. The silicon hinge has the following properties and dimensions: modulus of elasticity $E = 170$ GPa, density $\varrho = 2329$ kg/m^3, width $w = 5\,\mu$m, length $L_{top} = 330\,\mu$m, $L_{bottom} = 290\,\mu$m, and thickness $h = 280$ nm. For more details, please refer to Fig. 13.

Figure 14(a) shows that both the left (blue curve ●) and right (red curve ✖) sides of the beam exhibit similar responses, indicating excellent symmetry and construction quality. The rocking mode of the carbon fiber beam is approximately 187 Hz.

This identification is supported by a comparison with the base or chip measurement (represented by the symbol **B**), which refers to a reference point on the fixed chip. The base measurement, included in the figure, allows for a direct comparison between the response of the movable beam and that of the fixed chip. Several peaks appearing in the base results are attributed to electromagnetic interference in the instrumentation. For instance, as previously discussed, the 60 Hz peak corresponds to environmental noise or electromagnetic interference, as it appears in both the base and beam measurements. This mode is also canceled out through signal subtraction during data analysis (Fig. 10), confirming that it is not a structural mode of the beam.

Further support for the identification of the 187 Hz peak as the first mode comes from Fig. 15, which shows that the rocking mode occurs at approximately 128.3 Hz. Although this simulated result from the COMSOL model is lower than the experimentally measured 187 Hz, it still confirms the expected mode order: the rocking mode precedes the beam bending mode.

Another piece of evidence supporting the identification of the 187 Hz peak as the rocking mode comes from Fig. 14(b). This frequency acts as the primary driver of the sensing elements' acoustic response. The response increases steadily up to this frequency and then remains relatively constant up to 500 Hz. While an ideal acoustic response would stay flat throughout the audible range, a decline is observed beyond 500 Hz, consistent with expected behavior beyond the rocking mode.

Additional confirmation that the 187 Hz mode corresponds to the rocking mode comes from analyzing the other modes shown in Fig. 14(a). The gray curve (represented by the symbol ⬠) shows the noise floor measurement at the middle point of movable carbon fiber beams or the center of the structure. The results indicate that at approximately 370 Hz, the structure experiences vertical motion corresponding to the first bending mode of the silicon hinge. This observation aligns well with the COMSOL model, which also predicts a frequency close to 365.5 Hz. This mode is also evident in the top hinge midpoint (green ✳) and bottom hinge midpoint (yellow ✽) curves, measured at the midpoint of the top and bottom hinges, respectively. The amplitude level of this mode is most pronounced at the center of the structure and decreases as one moves from the center towards the hinges. This trend is clearly demonstrated by comparing the middle point curve (gray ⬠) with the top hinge midpoint (green ✳) and bottom hinge midpoint (yellow ✽) curves, showing a decrease in vibration amplitude from the midpoint to the hinges.

Together, these observations confirm that the 187 Hz mode corresponds to the rocking mode of the carbon fiber beam, and the 370 Hz mode corresponds to the first bending mode of the silicon hinge.

There is a mode observed at a frequency of 3.9 kHz, which could correspond to the second bending mode of the hinge. However, this mode is predicted to occur around 1.2 kHz in the COMSOL model, indicating a discrepancy with the experimental results. It is important to consider that these samples are handmade, lack perfect symmetry, and are glued together, which likely contributes to the mismatch between the COMSOL model and the actual measurements.

Two additional modes around 23 and 29.7 kHz, predicted by the COMSOL model as the third and fourth bending modes of the hinge, can also be identified in the experimental results. Beyond 10 kHz, the presence of numerous modes makes it impractical to discuss each in

J. Acoust. Soc. Am. **158** (2), August 2025

Karimi *et al.*   911

detail, so the focus is placed on the significant ones. The next important mode is the second bending mode of the movable carbon fiber beams, observed around 33 kHz in the left (blue ●) and right (red ✖) curves. This mode is also predicted at approximately 32.9 kHz by the COMSOL model, showing good agreement. Other modes are observed in the blue ●, red ✖, green ❋, and yellow ✳ curves around 6.5 and 7.8 kHz. However, the COMSOL model predicted in-plane modes at these frequencies, so they were not shown in Fig. 15 as they are not the focus of our study. It should be noted that while the structure also has in-plane modes, they are not included in this analysis. Given that the structure is handmade and not perfectly symmetric, these in-plane modes might slightly convert to out-of-plane modes, which is the reason they are detected by the laser vibrometer as out-of-plane modes.

Comparing the results depicted in Fig. 14(a) with that in Fig. 6(a) (the single carbon fiber sample held with a soft hinge and having less surface area), it is evident that Fig. 14(a) exhibited a significant reduction in the thermal noise floor level for almost all frequencies. Specifically, for the rocking mode frequency of the carbon fiber beam, the noise floor level decreases from approximately 8.2×10^{-4} (mm/s/$\sqrt{\text{Hz}}$) for Fig. 6 to 4.7×10^{-4} (mm/s/$\sqrt{\text{Hz}}$) for Fig. 14, which represents approximately a 1.8 times reduction. This notable improvement suggests that increasing the surface area enhances the damping of the structure due to viscous forces, consequently reducing the noise floor level across the frequencies. In order to see this comparison in detail, along with other comparisons, all samples will be compared together in Fig. 19 to provide a comprehensive view of the effectiveness of different parameters on the thermal noise floor, acoustic response, and pressure-referred noise.

On the other hand, Fig. 14(b) demonstrates that both sides of the beam exhibit similar responses across the 100 Hz to 10 kHz range, confirming the structure's well-constructed and balanced nature. The structure's effective response to low-frequency sounds is likely due to its driving mode occurring at approximately 180 Hz. In Fig. 14(c), the phase response indicates that the left and right sides of the beam are out of phase within the same frequency range.

This phase difference suggests that sound enters the cavity through the right side (Leading Edge) and exits through the left side (Trailing Edge), highlighting the directional nature of the structure's acoustic response.

2. Second prototype

In the next prototype, efforts were made to increase the surface area of the movable structure to determine if the thermal noise floor could be further reduced. This iteration utilized a single piece of silicon structure manufactured through silicon microfabrication techniques, selected as the movable beam.[33] The silicon structure's original hinges were replaced with soft hinges that were used in the previous samples, and then transferred to the same size cavity in order to have a consistent comparison with previous samples. Figure 16 depicts a teeter-totter microphone design featuring a single piece of silicon as the movable element. This element is coupled at both ends with a carbon fiber stiffener and held within a cavity by very thin silicon hinges at the top and bottom. Figure 16(a) shows the design without dimensions using microscope backlighting, in order to enhance visibility and provide a clearer view of the structure, while Fig. 16(b) provides detailed dimensions using microscope front lighting. The single piece of silicon has width $w = 700\ \mu\text{m}$, length $L = 1250\ \mu\text{m}$, and thickness $h = 5\ \mu\text{m}$. The silicon hinges dimensions are: width $w = 5\ \mu\text{m}$, length $L_{top} = 200\ \mu\text{m}$, $L_{bottom} = 150\ \mu\text{m}$, and thickness $h = 280\ \text{nm}$. For more details, please refer to Fig. 16.

Figures 17(a)–17(c) present the following characteristics of the teeter-totter microphone across various frequencies: (a) thermal noise floor response, (b) acoustic response, and (c) phase response. This innovative design features a single piece of silicon as the movable element, which is strengthened on both sides with carbon fiber stiffeners and equipped with very thin silicon hinges within the cavity structure. The thermal noise floor is measured across a frequency range of 50 Hz to 100 kHz to encompass all relevant modes, while the acoustic response data is concentrated within the 100 Hz to 10 kHz range, which is of primary
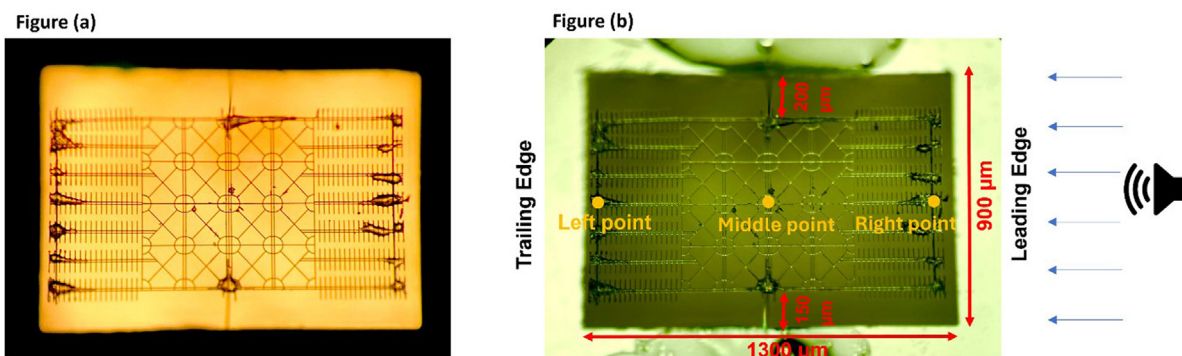

FIG. 16. Presents a teeter-totter microphone design with a single piece of silicon as the movable element, coupled at both ends with a carbon fiber stiffener, and secured within a cavity by very thin silicon hinges at the top and bottom, (a) shows the design without dimensions using microscope backlighting, while (b) provides detailed dimensions using microscope front lighting.
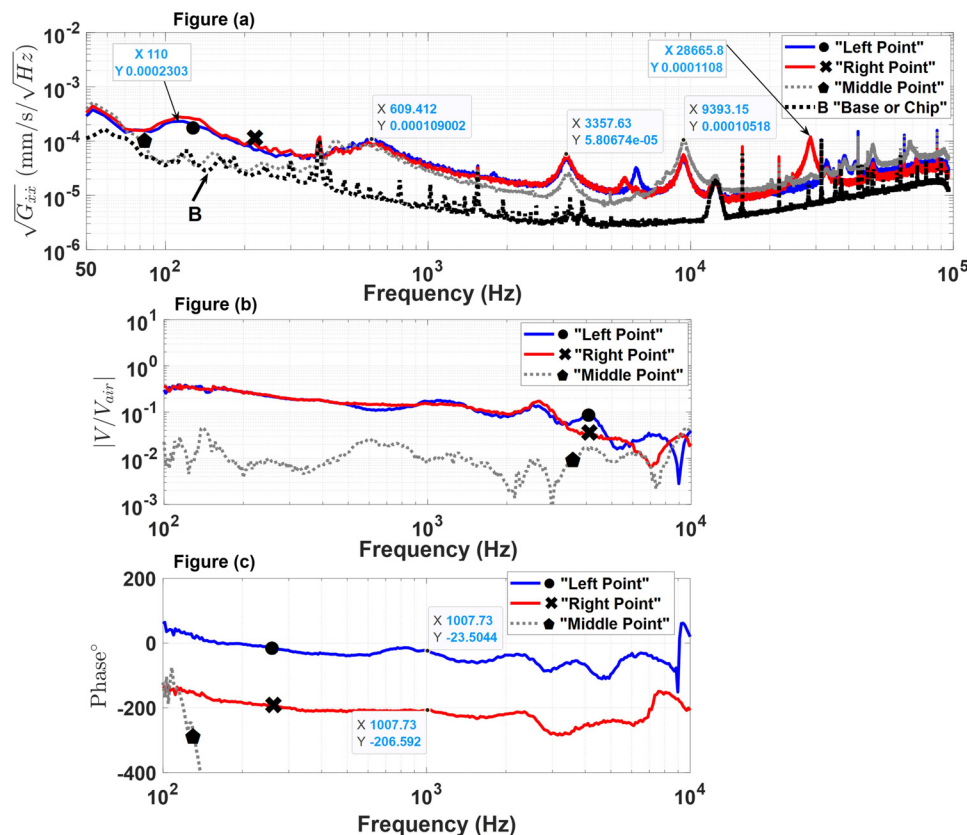
FIG. 17. Explains the (a) thermal noise floor response, (b) acoustic response, and (c) phase response of a teeter-totter microphone design with a single piece of silicon as the movable element, coupled at both ends with a carbon fiber stiffener, and held within a cavity by very thin silicon hinges across various frequencies.

interest. In Fig. 17(a), both the left (blue ●) and right (red ✖) sides of the beam exhibit similar responses, indicating a high level of symmetry and construction precision. The rocking mode of the silicon structure is approximately 110 Hz.

Comparing this result with the one depicted in Fig. 14, it becomes apparent that Fig. 17 shows a noticeable reduction in the thermal noise floor level for almost all frequencies. This enhancement suggests that the increased surface area further increases the damping of the structure due to viscous forces, consequently reducing the noise floor level. To explore this and other comparisons in greater detail, all samples will be analyzed together in Fig. 19, offering a complete overview of how various parameters impact the thermal noise floor, acoustic response, and pressure-referred noise.

The gray dotted curve (represented by symbol ⬟) illustrates the noise floor measurement taken at the middle point of the movable silicon structure. Observations suggest that around 610 Hz, the structure exhibits vertical movement, aligning with the first bending mode of the silicon hinge. There are modes observed at frequencies of 3.3 and 9.3 kHz, which could correspond to the second and third bending modes of the hinge, respectively. The next important mode is the second bending mode of the movable element, observed around 29 kHz in the left (blue ●) and right

(red ✖) curves. Since this sample is handmade and glued together, achieving a perfect shape is difficult. The resulting lack of perfect symmetry likely contributes to the presence of extra modes. Therefore, it is impractical to discuss each mode in detail, so the focus was placed on the notable ones.

Figure 17(b) illustrates a uniform response across both sides of the beam throughout the frequency range of 100 Hz to 10 kHz, affirming the well-engineered and balanced design of the structure. The structure's proficiency in handling low-frequency sounds is attributed to its resonant mode occurring at a relatively low frequency of approximately 110 Hz. The gray dotted curve (⬟), which represents the acoustic measurement at the midpoint of the movable silicon structure, indicates a lack of response at the center, suggesting that sound enters through the leading edge and exits through the trailing edge of the structure. In Fig. 17(c), the phase response reveals a phase discrepancy between the left and right sides of the silicon structure within the same frequency spectrum. This phase discrepancy reinforces the notion that sound enters through the right side and exits through the left side, emphasizing the directional aspect of the structure's acoustic response.

Now, it is time to synthesize the results obtained thus far to make meaningful comparisons. For better clarity, all samples are depicted together in Fig. 18. Figure 18(a) is labeled with the legend "movable single carbon fiber beam"
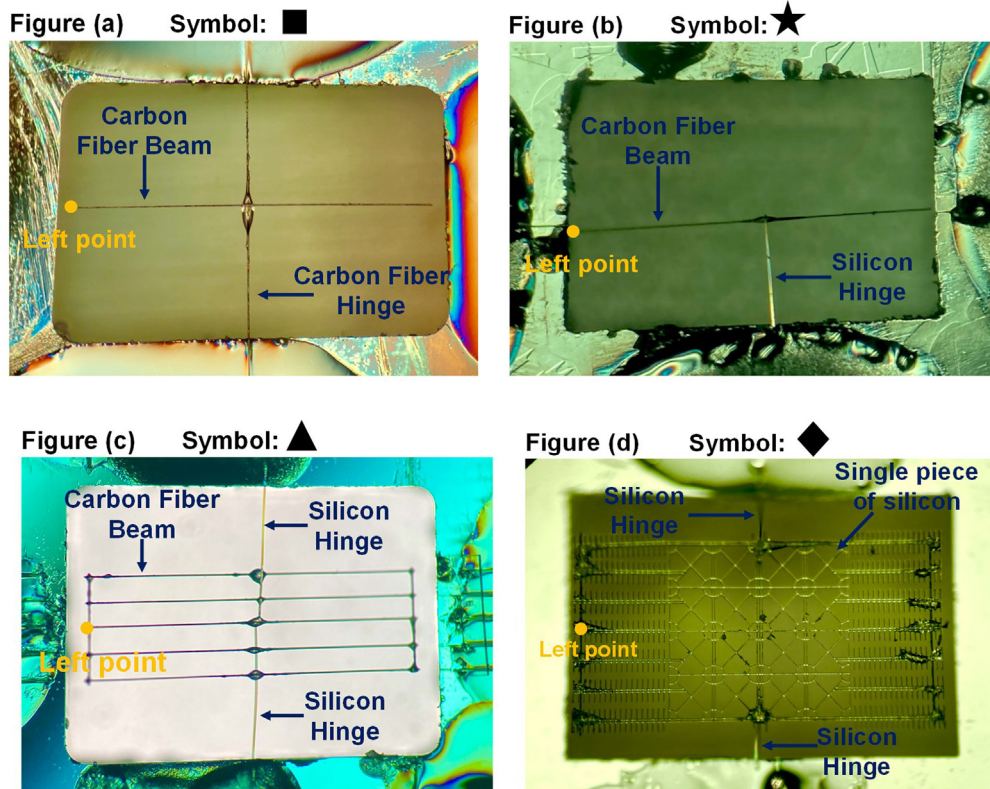
FIG. 18. Comparative Analysis of sample Configurations. (a) "movable single carbon fiber beam" and "single carbon fiber hinge" with symbol ■, (b) "movable single carbon fiber beam" and "one soft hinge" with symbol ★, (c) "5 movable carbon fiber beams" and "two soft hinge" with symbol ▲, (d) "movable single piece of silicon structure" and "two soft hinge" with symbol ◆.

and "single carbon fiber hinge," represented by the symbol ■. Figure 18(b) is labeled "movable single carbon fiber beam" and "one soft hinge," represented by the symbol ★. Figure 18(c) is labeled "5 movable carbon fiber beams" and "two soft hinges," represented by the symbol ▲. Finally, Fig. 18(d) is labeled "movable single piece of silicon structure" and "two soft hinges," represented by the symbol ◆.

Figure 19(a) the thermal noise floor response, Fig. 19(b) the acoustic response, and Fig. 19(c) the pressure-referred noise of a teeter-totter microphone design for different samples have been made so far across various frequencies. In this figure, only the left point of different samples was brought to do the comparison since the left and right sides have similar responses. In Fig. 19(a), comparing the blue curve (representing a design with carbon fiber for both the movable beam and hinge, symbolized by ■) with the red curve (representing a design with carbon fiber for the movable element and a very thin silicon hinge, symbolized by ★), it can be observed that softening the hinge of the structure results in a significant drop in the rocking mode frequency from 6 kHz to 150 Hz. This is a tremendous reduction in frequency for the rocking mode. Since the first bending mode of the movable beam is determined by its size and properties, which remain constant between the two designs, the first beam bending mode stays almost at the same frequency. Moreover, the comparison between the red curve (design with a carbon fiber for movable

element and a very thin silicon hinge, symbolized by ★) and the green curve (design with five carbon fibers for the movable element, strengthened at both sides with stiffeners, and two thin silicon hinges on the top and bottom of the cavity, symbolized by ▲) reveals that increasing the surface area of the structure leads to a substantial reduction in the thermal noise floor level for the rocking mode frequency of the carbon fiber beam. Specifically, for the rocking mode frequency of the carbon fiber beam, the noise floor level drops from approximately 8.2×10^{-4} (mm/s/$\sqrt{Hz}$) for the red curve ★ to 4.7×10^{-4} (mm/s/$\sqrt{Hz}$) for the green curve ▲, which represents approximately a 1.8 times reduction. This significant improvement suggests that increasing the surface area enhances the damping of the structure due to viscous forces, thereby effectively reducing the noise floor level for the rocking mode frequency. To further analyze the impact of increasing the surface area on the noise floor level, the green curve ▲ is compared with the yellow curve (design with a single piece of silicon for the movable element, coupled at both ends with a carbon fiber stiffener, and two thin silicon hinges at the top and bottom, symbolized by ◆). It can be observed that the thermal noise floor level drops across almost all frequencies. This observation supports the conclusion that further increasing the surface area continues to reduce the noise floor level, confirming that enhanced damping due to viscous forces leads to a decrease in the noise floor.

914   J. Acoust. Soc. Am. **158** (2), August 2025
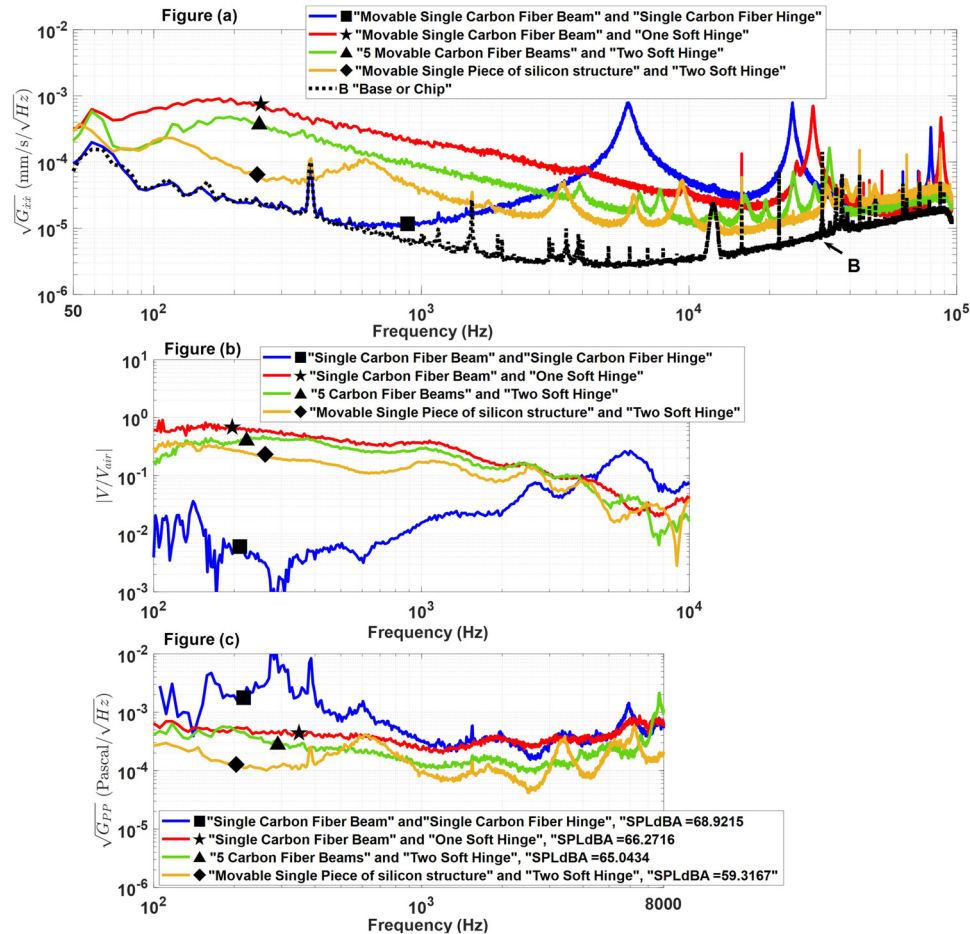
Karimi *et al.*

FIG. 19. Demonstrates the (a) thermal noise floor response, (b) acoustic response, and (c) phase response of a teeter-totter microphone design for different samples across various frequencies.

From Fig. 19(b), by comparing the blue curve (design with carbon fiber for both the movable beam and hinge, symbolized by a ■) with the other curves, it is evident that when the rocking mode frequency drops to a lower range, the sample's response to sound improves significantly. This is because this mode is the driving mode that causes the sample to respond to sound. It was predicted that increasing the surface area would enhance the acoustic response. However, it is important to note that the structures are attached by glue, which adds weight. This explains why the red curve ★ shows a better response compared to the others, despite having a smaller surface area, because it is lighter. Therefore, it is predicted that by increasing the surface area while keeping the structure reasonably light, the acoustic response will improve further.

Figure 19(c) indicates the pressure-referred noise of various teeter-totter microphone designs across different frequencies.

When comparing different structures, it is clear that the yellow curve ◆ exhibits the lowest pressure-referred noise, indicating better performance as a sensor. For instance, the blue curve ■ has a pressure-referred noise level of 68.9 SPLdBA, whereas the yellow curve ◆ has a significantly lower level at 59.3 SPLdBA. Although these noise levels are

higher than what is typically expected for a practical microphone, this represents an initial design. The focus of this study is to explore which parameters are most critical in determining the noise floor, paving the way for further optimization in future iterations.

This result confirms that by softening the hinge, decreasing the rocking mode to a lower frequency, and increasing the surface area while maintaining a reasonable structure weight, as well as keeping the first beam bending mode at a higher frequency out of the hearing threshold, the sensor's performance improves significantly. The yellow curve's design ◆ exemplifies this optimized approach, achieving an improved balance of low noise and high sensitivity among the tested samples.

III. CONCLUSIONS

This study presents the development and experimental analysis of a bio-inspired teeter-totter low-noise velocity-sensitive microphone. Through the construction of several micro-scale prototypes and systematic modification of key structural elements, valuable insights into optimizing microphone performance have been gained. The experimental results highlight the importance of several key factors as follows:

J. Acoust. Soc. Am. **158** (2), August 2025

Karimi *et al.*   915

- By softening the rotational hinge, the rocking mode of the movable beam was found to drop dramatically to a lower frequency; consequently, decreasing the thermal noise floor and improving acoustic response. This is significant as the rocking mode is the driving mode that causes the structure to respond to sound.
- Increasing the surface area of the movable structure was observed to decrease the thermal noise floor level. This occurs because the damping of the structure due to viscous forces increases, consequently reducing the noise floor level. Additionally, to achieve better acoustic response, it was determined that maintaining a minimal structure weight while increasing the surface area is important, as predicted.
- Keeping the first beam bending mode frequency above the desired frequency range was identified as crucial. Minimizing the number of extra modes within the frequency range of hearing is necessary to improve microphone performance.
- In general, it was discovered that by softening the rotational hinge, increasing the surface area of the movable structures while keeping their weight light, and maintaining the first beam bending mode above the desired frequency range while preventing extra modes within this range, the thermal noise floor could be lowered and acoustic response improved. Consequently, the pressure-referred noise decreased, potentially resulting in improved overall sensitivity of the microphone.

The findings from this research provide crucial guidelines for designing teeter-totter velocity-sensitive microphones. By understanding and implementing these key modifications, better-performing microphones can be achieved, which are essential for various applications in the audio and communication industries. The bio-inspired approach and experimental methodologies outlined in this study pave the way for future advancements in velocity-sensitive microphone technology, promising improved noise performance and acoustic sensitivity.

ACKNOWLEDGEMENTS

AUTHOR DECLARATIONS
Conflict of Interest

The authors have no conflicts to disclose.

DATA AVAILABILITY

The data that support the findings of this study are available within the article.

[1] R. N. Miles, M. Farahikia, S. Leahy, and A. A. Aziz, "A flow-sensing velocity microphone," in *Proceedings of the 2019 IEEE Sensors* (2019), pp. 1–4.

[2] R. Miles, "Most animals hear acoustic flow instead of pressure; we should too," J. Acoust. Soc. Am. **145**, 1698 (2019).

[3] J. Tautz and H. Markl, "Caterpillars detect flying wasps by hairs sensitive to airborne vibration," Behav. Ecol. Sociobiol. **4**, 101–110 (1978).

[4] M. A. Landolfa and G. A. Jacobs, "Direction sensitivity of the filiform hair population of the cricket cereal system," J. Comp. Physiol. A **177**, 759–766 (1995).

[5] J. Tautz, "Reception of particle oscillation in a medium—An unorthodox sensory capacity," Naturwissenschaften **66**, 452–461 (1979).

[6] T. Shimozawa, T. Kumagai, and Y. Baba, "Structural scaling and functional design of the cercal wind-receptor hairs of cricket," J. Comp. Physiol. A **183**, 171–186 (1998).

[7] F. G. Barth, U. Wastl, J. A. C. Humphrey, and R. Devarakonda, "Dynamics of arthropod filiform hairs. II. Mechanical properties of spider trichobothria (*Cupiennius salei*)," Philos. Trans. R. Soc. B **340**, 445–461 (1993).

[8] G. Menda, E. I. Nitzany, P. S. Shamble, A. Wells, L. C. Harrington, R. N. Miles, and R. R. Hoy, "The long and short of hearing in the mosquito *Aedes aegypti*," Curr. Biol. **29**, 709–714 (2019).

[9] R. N. Miles, D. Robert, and R. R. Hoy, "Mechanically coupled ears for directional hearing in the parasitoid fly *Ormia ochracea*," J. Acoust. Soc. Am. **98**, 3059–3070 (1995).

[10] D. Robert, R. N. Miles, and R. R. Hoy, "Directional hearing by mechanical coupling in the parasitoid fly Ormia ochracea," J. Comp. Physiol. A **179**, 29–44 (1996).

[11] A. C. Mason, M. L. Oshinsky, and R. R. Hoy, "Hyperacute directional hearing in a microscale auditory system," Nature **410**, 686–690 (2001).

[12] D. Robert and U. Willi, "The histological architecture of the auditory organs in the parasitoid fly *Ormia ochracea*," Cell Tissue Res. **301**, 447–457 (2000).

[13] A. C. Mason, "Cues for directional hearing in the fly *Ormia ochracea*," Front. Ecol. Evol. **9**, 679064 (2021).

[14] R. Bauer, Y. Zhang, J. C. Jackson, W. M. Whitmer, W. O. Brimijoin, M. A. Akeroyd, D. Uttamchandani, and J. F. C. Windmill, "Housing influence on multi-band directional MEMS microphones inspired by *Ormia ochracea*," in *Proceedings of IEEE Sensors 2016* (2016), pp. 1–3.

[15] R. Bauer, Y. Zhang, J. C. Jackson, W. M. Whitmer, W. O. Brimijoin, M. A. Akeroyd, D. Uttamchandani, and J. F. C. Windmill, "Influence of microphone housing on the directional response of piezoelectric MEMS microphones inspired by *Ormia ochracea*," IEEE Sens. J. **17**, 5529–5536 (2017).

[16] A. Ishfaque and B. Kim, "Fly Ormia ochracea-inspired MEMS directional microphone: A review," IEEE Sens. J. **18**, 1778–1789 (2017).

[17] H. Liu, M. Yu, and X. Zhang, "Biomimetic optical directional microphone with structurally coupled diaphragms," Appl. Phys. Lett. **93**, 243902 (2008).

[18] R. N. Miles and R. R. Hoy, "The development of a biologically-inspired directional microphone for hearing aids," Audiol. Neurotol. **11**, 86–94 (2006).

[19] R. N. Miles, Q. Su, W. Cui, M. Shetye, F. L. Degertekin, B. Bicen, C. Garcia, S. Jones, and N. Hall, "A low-noise differential microphone inspired by the ears of the parasitoid fly *Ormia ochracea*," J. Acoust. Soc. Am. **125**, 2013–2026 (2009).

[20] Y. Zhang, R. Bauer, J. C. Jackson, W. M. Whitmer, J. F. C. Windmill, and D. Uttamchandani, "A low-frequency dual-band operational microphone mimicking the hearing property of *Ormia ochracea*," J. Microelectromech. Syst. **27**, 667–676 (2018).

[21] Y. Zhang, R. Bauer, W. M. Whitmer, W. O. Brimijoin, D. Uttamchandani, J. F. C. Windmill, and J. C. Jackson, "Development of a biologically inspired MEMS microphone," in *Proceedings of the 2017 IEEE Sensors* (2017), pp. 1–3.

[22] Y. Zhang, J. F. C. Windmill, and D. Uttamchandani, "Biomimetic MEMS directional microphone structures for multi-band operation," in *Proceedings of IEEE Sensors 2014* (2014), pp. 440–443.

[23] R. N. Miles, W. Cui, Q. Su, and D. Homentcovschi, "A MEMS low-noise sound pressure gradient microphone with capacitive sensing," J. Microelectromech. Syst. **24**, 241–248 (2015).

[24] A. Rahaman and B. Kim, "Sound source localization by Ormia ochracea-inspired low-noise piezoelectric MEMS directional microphone," Sci. Rep. **10**, 9545 (2020).

[25]J. Zhou, J. Lai, G. Menda, J. A. Stafstrom, C. I. Miles, R. R. Hoy, and R. N. Miles, "Outsourced hearing in an orb-weaving spider that uses its web as an auditory sensor," Proc. Natl. Acad. Sci. **119**, e2122789119 (2022).

[26]J. Zhou and R. N. Miles, "Sensing fluctuating airflow with spider silk," Proc. Natl. Acad. Sci. U.S.A. **114**, 12120–12125 (2017).

[27]M. Karimi, J. Lai, W. Cui, C. Ke, and R. N. Miles, "The influence of fluid boundary conditions on bio-inspired acoustic flow sensor," J. Acoust. Soc. Am **157**(4), 3045–3056 (2025).

[28]J. Lai, M. Farahikia, Z. Liu, Y. Yiang, C. Ke, and R. N. Miles, "Effect of size on the thermal noise and acoustic response of viscous-driven microbeams," J. Acoust. Soc. Am. **155**, 2561–2576 (2024).

[29]J. Lai, Z. Liu, M. Karimi, M. Farahikia, W. Cui, J. Pourghader, S. Aghazadeh, C. Ke, and R. Miles, "A small cavity for detecting sound-induced flow," J. Acoust. Soc. Am. **157**, 29–42 (2025).

[30]M. I. Younis, *MEMS Linear and Nonlinear Statics and Dynamics* (Springer, New York, 2011).

[31]R. N. Miles, *Physical Approach to Engineering Acoustics* (Springer, New York, 2020).

[32]J. Lai, M. Karimi, and R. N. Miles, "Methods for accurate acoustic characterization with ultra-low noise and minimal effect from acoustic reflections," EngrXiv (2023).

[33]J. Pourghader, W. Cui, J. Lai, M. Farahikia, C. Ke, M. Karimi, and R. N. Miles, "Bio-inspired Flow-Sensing Capacitive MEMS Microphone," J. Acoust. Soc. Am. **157**, 3897–3906 (2025).

J. Acoust. Soc. Am. **158** (2), August 2025

Karimi *et al.*   917